M.S. THESIS

A numerical analysis of a correlation of swirl number in a coannular swirl injector

동심환형 Swirl injector에서의 Swirl number 에 대한 새로운 관계식의 제안 및 수치적 분석

BY

Jaehoon Choi

AUGUST 2017

DEPARTMENT OF AEROSPACE AND
MECHANICAL ENGINEERING
COLLEGE OF ENGINEERING
SEOUL NATIONAL UNIVERSITY

M.S. THESIS

A numerical analysis of a correlation of swirl number in a coannular swirl injector

동심환형 Swirl injector에서의 Swirl number 에 대한 새로운 관계식의 제안 및 수치적 분석

BY

Jaehoon Choi

AUGUST 2017

DEPARTMENT OF AEROSPACE AND
MECHANICAL ENGINEERING
COLLEGE OF ENGINEERING
SEOUL NATIONAL UNIVERSITY

A numerical analysis of a correlation
of swirl number in a coannular swirl injector

동심환형 Swirl injector에서의 Swirl number
에 대한 새로운 관계식의 제안 및 수치적 분석

지도교수 Hyungrok Do

이 논문을 공학석사 학위논문으로 제출함

2017 년 7 월

서울대학교 대학원

기계항공공학부

Jaehoon Choi

Jaehoon Choi의 공학석사 학위논문을 인준함

2017 년 7 월

위 원 장	Prof. Sang Ken Kauh
부위원장	Porf. Hyungrok Do
위 원	Prof. Charn-Jung Kim

Abstract

Gas turbine combustors using lean-premixed combustion often utilizes a swirling flow to generate a central-toiroidal recirculation zone (CTRZ) for flame stabilization. The characteristics of a CTRZ, such as the volume of a CTRZ, can be predicted by the swirl number at the combustor inlet (or the exit of the swirl injector). In the present study, a new numerical model for the swirl number is derived to estimate the swirl number at the end of a swirl-injector pipe, especially for the pipe with a variable cross-sectional area, where existing formulas cannot be applied accurately. First, a new one-dimensional model to predict the swirl decay rate is proposed to estimate the swirl intensity at the end of the swirl injector. Next, the proposed model is validated with the CFD simulations in various swirl injectors. As a result of validation, the proposed model is confirmed to be in good agreement with the results in CFD simulations. In Chapter 4, the variation of decay rate of swirl with the factors affecting the swirl is analyzed through the proposed model. It is found that the decay rate of swirl decreases as the inlet Reynolds number increases and initial swirl intensity decreases. It is also has been shown that a straight annular pipe can minimize the decay rate of swirl when having a specific the ratio of inner radius to outer radius of a swirl injector. This value is estimated as about 0.35 according to the proposed model. It is expected that the proposed model of variation of swirl number is very useful for the selection of appropriate swirler to obtain the desired swirl number in swirl injectors.

Keywords: Swirl number, Decay rate of swirl, Swirl injector, Swirl-stabilized burner

Student Number: 2015-20758

Contents

List of Figures

List of Tables

Chapter 1

Introduction

1.1 Motivation and objectives

Many conventional gas turbines used the combustors based on the diffusion flames because of their proved performance and stability. The gas turbines of this type have an issue in emitting large amount of thermal NO_x. Therefore, they have difficulties to satisfy the recent regulations for pollutant emission [1,8]. Therefore, new concepts of combustion technology have been introduced for environmentally friendly combustion in the gas turbines [23]. Among them, lean-premixed (LPM) combustion is regarded as one of the most viable concepts for clean and efficient combustion in the gas-turbines [17]. The LPM combustion uses fuel-lean mixture to reduce the flame temperature. In LPM combustion, the fuel and air are premixed at the upstream of the combustor and burnt with excess air in the combustion zone. The flame temperature of a LPM combustor is consequently lower than that of the diffusion flame.

Many LPM combustors employ the swirl injectors that produce a swirling

flow [16] to stabilize the fuel-lean flame. The swirling flow forms a central toroidal recirculation zone (CTRZ), that recirculates the heat and active chemical species to the root of the flame. The CTRZ can be utilized as a primary mechanism for flame stabilization in the LPM combustors [17, 36].

The most commonly used parameter to characterize the swirling flows is the swirl number [2, 32], defined as

$$S \equiv \frac{G_\theta}{r_o G_x}$$

where S is the swirl number, G_θ is the angular momentum, G_x is the axial momentum, and r_o is the outer radius of the pipe.

In a swirl-stabilized burner, it is important to know the swirl number at the exit of the swirl injector (or burner inlet) in order to understand the dynamics of the flow and flame. For example, it was observed that a CTRZ is formed only at above a critical swirl number (> 0.6) in the previous experimental [4] and numerical studies [34]. The shape and axial position of a CTRZ is known to be a function of the swirl number [35]. Flame stabilization/formation can therefore be analyzed using the swirl number in a quantitative manner. The unsteady flow oscillation (or combustion instability) that is a common issue in the LPM combustors [25] can be characterized by the swirl number as well. Several previous studies [11, 12, 24] showed that there are seven different types of vortex breakdown phenomena parametrized by the Reynolds and swirl numbers. Similarly, it was mentioned in [35] that large-scale unsteady motions such as precession of the vortex core and vortex breakdown are affected strongly by the swirl number and burner geometry. Regarding the flame stability in combustion systems, a number of previous studies investigated the effect of a swirl on flame dynamics [5, 14, 15, 37]. Tangirala et al. [37] investigated the properties of strongly swirling flames ($S > 1$) with the swirl numbers up to

4. Their results showed that mixing and flame stability can be improved by increasing the swirl number up to approximately the unity, beyond which a further increase reduces the turbulence level and flame stability. Consequently, an appropriate range of the swirl strength for their swirl-stabilized flames could be established.

Figure 1.1 The geometry of the coannular swirl injector having a variable cross-sectional area.

There are a few empirical correlations for the swirl number reported in the literature. For a flat-vane axial swirler, the equation of Beer and Chigier [2] is commonly used. Sheen et al. [32] proposed a correlation of the swirl number for a radial-type swirler. These correlations show an acceptable approximation of the swirl number close to a swirler. Nevertheless, these equations cannot reflect the variation of the swirl number along the axial direction, when there is a developing zone between the swirler and the nozzle exit. An example of this case is shown in figure. 1.1. A swirl injector of this type is useful because it enables a flexible control over the inlet velocity and can produce a more uniform swirl flow with the swirler placed at an upstream of the nozzle. Besides, a partially premixed mixture can be controlled precisely by placing the fuel inlet holes at an upstream location of the nozzle exit. In this case, it is very useful to predict the swirl number at the exit for a given swirler configuration such as the design,

location, flow rate etc. for the design process. In order to evaluate a possibility of an existing empirical correlation for the swirl number, a large eddy simulation (LES) was performed for the geometry in figure. 1.1. The swirl numbers along the axial direction from the correlation of [2] and the present LES is shown in figure 1.2, which shows a large discrepancy except for $x/D = 0$ right after the swirler. This shows that the existing correlation is not suited well to an analysis of the present swirl injector. Specifically, it does not consider the physical effects of a variable cross-sectional area and a decay of the swirl number via diffusion, etc. To our knowledge, there is no empirical or theoretical model to predict the variation of the swirl number correctly for the swirl injector with a developing zone.

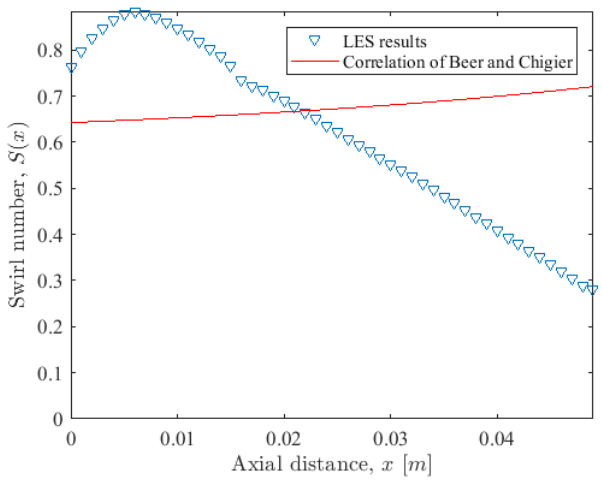

Figure 1.2 Plot of the swirl numbers along the axial direction in figure 1.1.

The purpose of the present study is to propose a new one-dimensional model that can predict the axial variation of the swirl number accurately in a swirl injector with a developing zone. A new numerical model is derived by extending the existing empirical correlations for swirlers considering a few physical effects

occurring inside the developing zone. A new model is applicable to a swirl injector with a varying cross-sectional area, for which the existing correlations cannot be applied correctly. The proposed model is validated against the results obtained by numerical simulations in various swirl injectors. A comparison with the previous studies is also carried out to confirm that the proposed equation can predict the swirl number at the nozzle exit, that is important to characterize the flow and flame stability in a swirl-stabilized burner.

1.2 Previous studies and background

Over the past decades, many studies has been conducted on the confined swirling flow in circular or annular pipe. Kitoh [21] conducted an experimental study on turbulent swirling flow in long pipe to identify the physics of swirl. The author showed that the swirling flow can be expressed as a sum of forced and free vortex motions. It is also found that the swirling flow has three regions along the radial position: wall, annular, and core regions. Especially in the near wall region, the velocity profile of the swirling flow was confirmed to be largely deviated from the logarithmic law. Also, they point out the highly anisotropic turbulence of the swirling flow. They derived the decay rate of swirl in exponential form and revealed that the exponents varies depending on the swirl intensity.

Fejer et al. [13] implemented the experiment for the decay of swirl using hot-wire anenometer. They revealed that the decay of swirl is clearly more rapid at the smaller inlet Reynolds number.

Frank and Sonju [22] approached the swirl decay rate of the turbulent swirling flow in pipe through analytic methods. The swirl equation, which is named by the authors, is derived from the Reynolds-averaged Navier-Stokes

equation through assumptions based on existing experimental results and the assumption of steady, incompressible and axisymmetric flows through the order of magnitude analysis. The swirl equation is analytically solved by separating variable technique. They assumed that the time-averaged axial velocity is independent to the radial position and the time-averaged azimuthal velocity has a profile of rigid body rotation. The eddy viscosity was obtained from the empirical correlation and assumed to be independent of radial position. The swirl decay rate obtained from the solution showed a good agreement with the experimental results. Moreover, the fact that the swirl decay rate decreases with increasing inlet Reynolds number was revealed.

Yao and Fang [40] obtained the analytic solutions of the swirl decay rate using the separation variable technique from the Navier-Stokes equation for laminar flow in circular straight pipe. Several analytic solutions were obtained through the assumption of radial shape of azimuthal velocity. They confirmed that the most important factor in the swirl decay rate is the wall shear stress from the fact that the difference between the swirl numbers obtained from the derived solutions are small enough. It was once again confirmed that the swirl decay rate decreases as the inlet Reynolds number increases.

Steenbergen and Voskamp [33] started from the angular momentum equation to investigate the swirl decay rate for turbulent weak swirling flow in pipe. The solution of swirl decay rate was expressed as the exponential form from the analysis. The exponents was determined through data-fitting with their laser Doppler velocimetry (LDV) results. They classified the swirl into three types with the radial profile shape of swirl velocity, but their results showed the decay rates of swirl are almost identical regardless of the types of swirl, at least for the weak swirling flow ($0 < S < 0.18$). They concluded that the important parameter for the decay of swirl is the friction factor (or wall friction) for

fully-developed flow.

There are also studies about the confined turbulent swirling flow in annular pipes. Wattendorf [38] investigated the effect of streamline curvature on the turbulent flow. They used curved channels of constant curvature and cross-sectional area to isolate the effect of streamline curvature. Their experimental results showed the turbulent viscosity is less than that for straight pipe near the convex wall (or inner wall) and greater than that for straight pipe near the concave wall (or outer wall). The turbulent viscosity near the outer wall is four times larger than that for the inner wall. The author explained these results with Reyleigh's stability criterion. Near the inner wall, the turbulence is suppressed due to the stabilizing effect because the gradient of the radial position of the local angular momentum is positive. On the other hand, the turbulence near the outer wall is strengthened by labilizing effect due to the negative gradient of the local angular momentum. An experimental study of Eskinazi and Yeh [10], who also conducted the similar experiment of Wattendorf, obtained the same results.

Scott [29] derived the equation for the swirl velocity ratio from a linearized swirl equation to a straight annular pipe in the form of a first-order Bessel function, with some assumptions such as in [22]. The plot of decay of swirl velocity is drawn from the derived equation with the assumption of a free-vortex type swirl. Their formula shows that the characteristics of initial free-vortex is rapidly lost as the flow progressed.

Scott and Risk [31] measured the turbulent swirling flow using isothermal air in a straight annular pipe with $r_i/R_0 = 0.4$. Their experiment has shown the hydrodynamic stability characteristics of the turbulent swirling flow by confirming that the turbulence near the outer wall is larger than turbulence near the inner wall in annular pipe as in [38]. The initial swirl having a free-

vortex nature in the inlet changed to that of a forced-vortex nature in the outlet regardless of the initial swirl intensity. Axial diffusivities are weakly influenced by swirl. They explained this result with the fact that the axial velocity profile is not significantly affected by swirl. In other study of Scott and Risk [30], they induced the swirl of forced vortex type in the same straight annular pipe. The major experimental work in [30] was focused on obtaining velocity profiles over the annular cross section at various axial locations along the pipe. The experimental results show that the swirl exhibits a forced vortex throughout the length of the pipe. In addition, in this study they divide the flow region into an outer region and an inner region and model a turbulent viscosity for each region.

Clayton and Morsi [6] generated a free vortex swirl in a straight annular pipe and measured time mean parameters such as mean velocities, swirl decay rate, static pressure, and flow angle. Similar to Scott's experimental results [31], it was confirmed that the swirl, which initially had the characteristics of free vortex nature, gradually became close to the characteristic of the forced vortex nature as the flow moves downstream. They also measured changes in swirl decay while changing the inlet swirl intensity, inlet Reynolds number, and r_i/R_0. Their results show that the decay rate of swirl increases with increasing initial swirl intensity, lower inlet Reynolds number, and r_i/R_0 from 0.51 to 0.61.

Chapter 2

A new one-dimensional model for streamwise evolution of swirl number

The swirl number is defined by momentum fluxes, that is by velocities as follows.

$$S = \frac{G_\theta}{r_o G_x} = \frac{\int_A \rho u w r dA}{r_o \int_A \rho u^2 dA} \tag{2.1}$$

where u is (time-averaged) axial velocity, w is (time-averaged) azimuthal velocity, and ρ is the fluid density.

With axisymmetric assumption, the velocities can be expressed only in terms of the radial and axial components.

$$u(x,r) = \bar{u}(x) \times fcn_1(r)$$
$$w(x,r) = \bar{w}(x) \times fcn_2(r)$$

The overbar denotes the mean over cross-sectional area. The fcn_1 and fcn_2 represent the radial distribution of the axial and the azimuthal velocities. These

functions can be reasonably expressed using the parabolic assumption for the laminar flow. For turbulent flow, there is no profile that can accurately represent for these functions from a theoretical standpoint. Therefore, in this study, it is assumed that the axial and azimuthal velocities have a uniform profile for turbulent flow. Even if there is swirling, it is reasonable to assume the flat profile for axial velocity except for the region close to the entrance where swirling is applied according to many studies [22, 31, 33]. The fcn_2 is usually modeled using profiles of free vortex and forced vortex. The main source term for angular momentum, however, is wall shear stress [33, 40]. Therefore, if we have an appropriate description of wall shear stress as in section 2.3, the flat-profile assumption in the r direction for the azimuthal velocity is an appropriate simplification in the decay rate of swirl from the viewpoint of modeling.

The $\bar{u}(x)$ can be simply described by the geometric relationship with the mass conservation.

$$\bar{u}(x) = \frac{A_0}{A_x}\bar{U}_0$$

where A_0 is the cross-sectional areas at the reference position, that is at the upstream of the swirler, A_x is the cross-sectional area at the axial position x, and $\bar{U}_0$ is the mean total velocity at the upstream of a swirler; $\bar{U}_0$ is mean axial velocity at the upstream of a swirler.

In the case of $\bar{w}(x)$, it can be obtained by describing an ordinary differential equation (ODE) for $\bar{w}(x)$ with the momentum conservation equation through Reynolds transport theorem (RTT).

2.1 Reynolds transport theorem (RTT)

In this study, ODE for $\bar{w}$ is expressed through linear momentum conservation as in other studies [22, 29, 40]. The linear momentum conservation has the advantage that it is relatively simple to describe source terms rather than an angular momentum conservation. Therefore, we use the linear momentum conservation in the tangential direction through RTT to establish ODE for the mean azimuthal velocity.

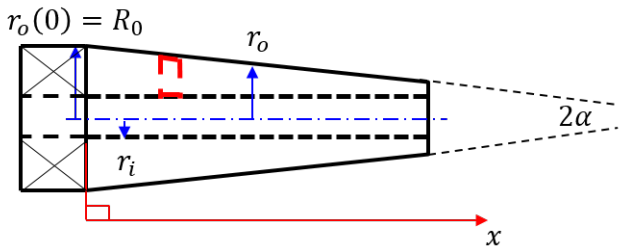

Figure 2.1 Coannular swirl injector.

Consider a coannular swirl injector as in figure 2.1. α is the converging angle of swirl injector. The outer radius, r_o can be expressed as $r_o(x) = R_0 - x\tan\alpha$ from a geometric relationship. R_0 is the outer radius of the swirler, and r_i is the inner radius of the annular pipe. Determine the control volume as the red dashed box in figure 2.1.

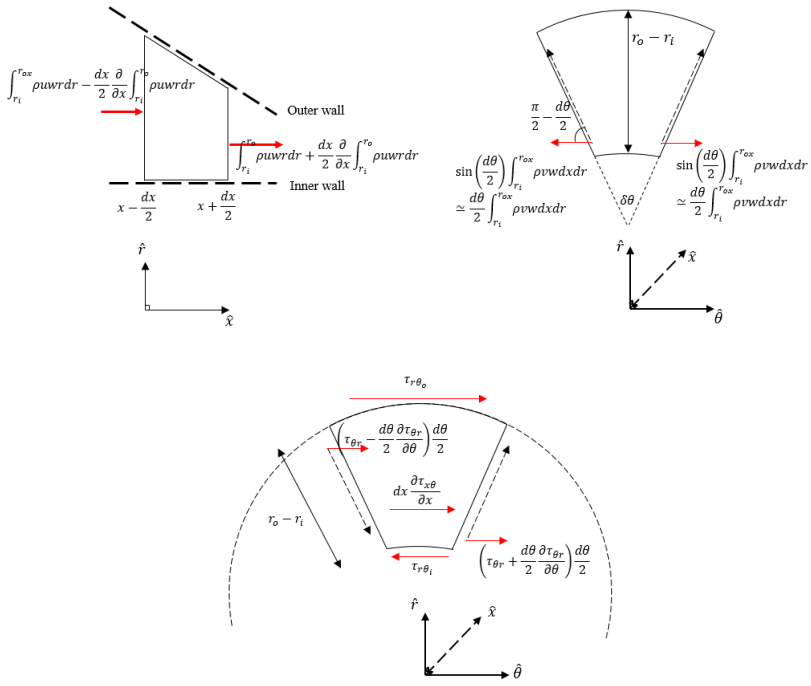

Figure 2.2 Schematics of fluxes through the control surfaces in RTT analysis: (1) momentum flux through x plane (top left); (2) momentum flux through θ plane (top right); and (3) tangential friction forces (bottom)

With the assumption of incompressible and axisymmetric flow, the linear momentum conservation can be written through RTT as below.

$$\frac{\partial}{\partial t}\int_{r_i}^{r_o}\rho uwrdr = -\frac{\partial}{\partial x}\int_{r_i}^{r_o}\rho uwrdr - \int_{r_i}^{r_o}\rho vwdr$$
$$+\frac{\partial}{\partial x}\left\{\int_{r_i}^{r_o} r\mu_{x\theta}^{eff}\frac{\partial w}{\partial x}dr\right\} + \int_{r_i}^{r_o}\mu_{r\theta}^{eff}\left(\frac{\partial w}{\partial r}-\frac{w}{r}\right)dr + \frac{r_o\tau_{r\theta_o}}{\cos\alpha} - \tau_{r\theta_i}r_i \quad (2.2)$$

where $\tau_{r\theta_o}$ and $\tau_{r\theta_i}$ are the tangential wall shear stresses on the outer and inner walls, respectively. $\mu_{x\theta}^{eff}$ and $\mu_{r\theta}^{eff}$ are the effective viscosities.

The term on the left-hand side of equation 2.2 represents the temporal change of the tangential momentum flux. The six terms on the right-hand side of equation 2.2 represent: (1) the advection of the tangential momentum flux through the x plane; (2) the advection of the tangential momentum flux through the θ plane; (3) the tangential friction on the x plane; (4) the tangential friction on the θ planes; (5) the tangential wall friction on the outer wall; and (6) the tangential wall friction on the inner wall.

The radial velocity, v can be regarded as zero for swirling flow in a straight annular pipe [21, 22, 29–31, 33, 40]. However, for a swirling flow in the annular pipe with a variable cross-sectional area, the radial velocity is greater than in the previous case. A description of the radial velocity is therefore needed for this case. The radial velocity can be estimated by the continuity equation in cylindrical coordinates.

$$rv = -\int r\frac{\partial u}{\partial x}dr \tag{2.3}$$

However, the distribution of radial velocity in the r direction from equation 2.3 never satisfies the no-slip conditions at both the outer and inner walls at the same time under the assumption of the flat profile of axial velocity. That is, if $v(r_i, x) = 0$ is satisfied, $v(r_o, x) = 0$ is not satisfied and vice versa. In this case, the methods of matched asymptotic expansions can be used for more accurate description of the radial velocity. However, in this study, the profile obtained directly from the equation 2.3 is used for simplicity. Since we deal with the swirl injector having a variable r_o, it is more realistic to consider $v(r_i, x) = 0$ as the boundary condition. Therefore, the (time-averaged) radial velocity can be described as

$$v = \frac{d\bar{u}}{dx}\left(\frac{r_i^2}{2r} - \frac{r}{2}\right)$$

Equation 2.2 can be simplified under the assumptions of the velocities described above for incompressible steady flow as follows.

$$0 = -\frac{d}{dx}\int_{r_i}^{r_o} \rho uwr dr - \int_{r_i}^{r_o} \rho vw dr + \frac{d}{dx}\left\{\int_{r_i}^{r_o} r\mu_{x\theta}^{eff}\frac{\partial w}{\partial x}dr\right\} + \int_{r_i}^{r_o} \mu_{r\theta}^{eff}\left(\frac{\partial w}{\partial r} - \frac{w}{r}\right)dr + \frac{r_o\tau_{r\theta_o}}{\cos\alpha} - \tau_{r\theta_i}r_i \tag{2.4}$$

Equation 2.4 is second-order ODE for mean azimuthal velocity. $\bar{w}(x)$ can be obtained by solving equation 2.4. For laminar flow, equation 2.4 can be expressed as

$$0 = -\frac{d}{dx}\int_{r_i}^{r_o} \rho uwr dr - \int_{r_i}^{r_o} \rho vw dr + \frac{d}{dx}\left\{\int_{r_i}^{r_o} r\mu\frac{dw}{dx}dr\right\} + \int_{r_i}^{r_o} \mu\left(\frac{\partial w}{\partial r} - \frac{w}{r}\right)dr + \frac{r_o\tau_{r\theta_o}}{\cos\alpha} - \tau_{r\theta_i}r_i \tag{2.5}$$

where μ is a molecular viscosity of fluid.

In the case of turbulent flow, equation 2.4 can be written as below.

$$0 = -\frac{d}{dx}\int_{r_i}^{r_o} \rho\bar{u}\bar{w}r dr - \int_{r_i}^{r_o} \rho v\bar{w} dr + \frac{d}{dx}\left\{\int_{r_i}^{r_o} r\mu_{x\theta}^{eff}\frac{d\bar{w}}{dx}dr\right\} - \int_{r_i}^{r_o} \mu_{r\theta}^{eff}\frac{\bar{w}}{r}dr + \frac{r_o\tau_{r\theta_o}}{\cos\alpha} - \tau_{r\theta_i}r_i \tag{2.6}$$

As described in previous studies [33, 40], the terms related to wall drag, $\tau_{r\theta_o}$ and $\tau_{r\theta_i}$ are the main source term of the decay of swirl, so more careful descriptions will be developed in section 2.3.

2.2 Non-dimensionalization

For turbulent flow, the analytic solution cannot be obtained because of the non-linearity of equation 2.6 and can only be solved numerically. Non-dimensionalization, therefore, proceeds in order to obtain more useful information.

Introducing the following dimensionless variables:

$$\hat{r}_o = \frac{r_o}{R_0}, \gamma = \frac{r_i}{R_0}, \hat{x} = \frac{x}{R_0}, \hat{r} = \frac{r}{R_0}$$
$$\hat{\bar{w}} = \frac{\bar{w}}{\bar{U}_0}, \hat{\bar{u}} = \frac{\bar{u}}{\bar{U}_0}, \hat{v} = \frac{v}{\bar{U}_0}, \hat{\bar{v}} = \frac{\bar{v}}{\bar{U}_0}, \hat{\bar{U}} = \frac{\bar{U}}{\bar{U}_0} = \sqrt{\hat{\bar{u}}^2 + \hat{\bar{w}}^2 + \hat{\bar{v}}^2}$$

With the dimensionless variables, equation 2.6 can be non-dimensionalized as

$$\begin{aligned} 0 = &-\frac{d}{d\hat{x}} \int_\gamma^{\hat{r}_o} \hat{\bar{u}}\hat{\bar{w}}\hat{r}d\hat{r} - \int_\gamma^{\hat{r}_o} \hat{v}\hat{\bar{w}}d\hat{r} + \frac{d}{d\hat{x}} \left\{ \frac{d\hat{\bar{w}}}{d\hat{x}} \int_\gamma^{\hat{r}_o} \left(\frac{\mu_{x\theta}^{eff}}{\rho \bar{U}_0 R_0} \right) \hat{r}d\hat{r} \right\} \\ &-\hat{\bar{w}} \int_\gamma^{\hat{r}_o} \left(\frac{\mu_{r\theta}^{eff}}{\rho \bar{U}_0 R_0} \right) \frac{1}{\hat{r}} d\hat{r} + \left(\frac{\tau_{r\theta_o}}{\rho \bar{U}_0^2} \right) \frac{\hat{r}_o}{\cos\alpha} - \left(\frac{\tau_{r\theta_i}}{\rho \bar{U}_0^2} \right) \gamma \end{aligned} \tag{2.7}$$

It is noted that the following dimensionless variables can be rearranged as follows.

$$\hat{r}_o = 1 - \hat{x}\tan\alpha$$

$$\hat{\bar{u}} = \frac{\bar{u}}{\bar{U}_0} = \frac{A_0}{A_x} = \frac{1-\gamma^2}{\hat{r}_o^2 - \gamma^2}$$

2.3 Description of the tangential wall shear stresses

Since the most important source term in decay of swirl is wall drag [33, 40], more careful descriptions for tangential wall friction are required to obtain a

better solution from equation 2.4. Therefore, the Moody friction factor is used to represent the wall shear stresses. The Moody friction factor is expressed either as a theoretical equation or as an equation fitted to the Moody chart. These equations are a simple way to calculate wall shear stress accurately [39].

Start from a laminar flow. For laminar flow in a circular pipe, the Moody friction factor, f can be written as

$$f = \frac{64}{Re_{D_h}}$$

where Re_{D_h} is the hydraulic Reynolds number, that is $Re_{D_h} = \frac{\rho \bar{U} D_h}{\mu} = \frac{\rho \bar{U} 2 r_o}{\mu}$ for a circular pipe. $\bar{U}$ is the mean total velocity.

This expression, however, is a formula for circular pipe, and the correction is needed to apply this formula to the annular pipe. According to Jones et al. [20], this correction can be accomplished by using effective laminar-diameter, D_{eff} instead of hydraulic diameter, D_h.

$$D_{eff} = (1/\zeta) D_h$$

The dimensionless term ζ is a correction factor for the hydraulic diameter, and is written for a concentric annular pipe as follows [39]

$$\zeta = \frac{(r_o - r_i)^2 (r_o^2 - r_i^2)}{r_o^4 - r_i^4 - \left(r_o^2 - r_i^2\right)^2 / \ln\left(r_o / r_i\right)} = \frac{\left(\hat{r}_o - \gamma\right)^2 \left(\hat{r}_o^2 - \gamma^2\right)}{\hat{r}_o^4 - \gamma^4 - \left(\hat{r}_o^2 - \gamma^2\right)^2 / \ln\left(1/\gamma\right)}$$

The friction factor for laminar flow in a concentric annular is then

$$f = \frac{64}{Re_{eff}} = \frac{64\zeta}{Re_{D_h}} \tag{2.8}$$

where Re_{eff} is the effective Reynolds number, and can be written as $Re_{eff} = \frac{\rho \bar{U} D_{eff}}{\mu} = \frac{\rho \bar{U} 2 (r_o - r_i)}{\zeta \mu}$ for an annular pipe.

For laminar flow, the assumption of the parabolic profile of the velocity components suggests that the total wall shear stresses in both the inner and outer walls is similar. That is

$$|\tau_{w_o}| = |\tau_{w_i}| = \tau_w = \frac{f}{8}\rho\bar{U}^2 \tag{2.9}$$

where τ_{w_o} is the total shear stress on the outer wall, and τ_{w_i} is the total shear stress on the inner wall, and $\bar{U} = \sqrt{\bar{u}^2 + \bar{w}^2 + \bar{v}^2}$ is mean total velocity.

Equation 2.4 requires tangential wall shear stresses instead of total wall shear stress, so the above description is insufficient to express the linear momentum conservation in the θ direction. The tangential wall shear stress can be obtained by multiplying the sine of flow angle by the total wall shear stress. Consider figure 2.3.

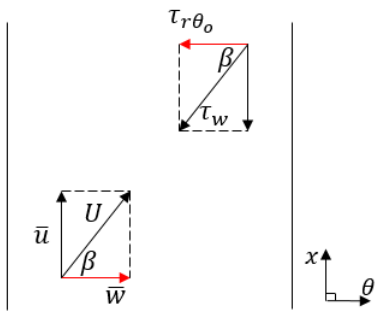

Figure 2.3 Computation of tangential wall shear stress.

If the total wall shear stresses is assumed to point into the direction of the mean bulk flow, we can simply compute the tangential wall shear stress by using the flow angle, $\frac{\pi}{2} - \beta$.

$$|\tau_{r\theta_o}| = |\tau_{r\theta_i}| = \tau_w \cos\beta = \frac{f}{8}\rho\bar{w}\bar{U} \tag{2.10}$$

Substituting the friction factor of equation 2.8, the terms associated with tangential wall friction in equation 2.4 can be described for a laminar flow.

The friction factor for turbulent flow in a circular pipe can be computed with Blasius formula, which is valid for the turbulent flow in a circular pipe with Reynolds number of 100,000 or less.

$$f = \frac{0.316}{Re_{D_h}^{0.25}}$$

The correction method in the concentric annular pipe described above can also be applied for turbulent flows as in laminar flows [39]. The friction factor of the turbulent flow in the annular pipe can then be expressed as

$$f = \frac{0.316}{Re_{eff}^{0.25}} = \frac{0.316}{\{(1/\zeta)Re_{D_h}\}^{0.25}}$$

In case of turbulent flows, the wall shear stresses should be distinguished from outer wall and inner wall, unlike laminar flows. This is related to the hydrodynamic stability of the turbulent swirling flow in annular pipes as pointed out in previous studies [7, 10, 30, 31, 38]. According to Rayleigh [27], the flows with $\frac{\partial}{\partial r}(wr) > 0$ are stable while the flows with $\frac{\partial}{\partial r}(wr) < 0$ are unstable. This is because that the particles in revolving motion tend to conserve their local angular momentum, wr. Consider the flow near the concave (or outer) wall in a curved channel. If the fluid in this region is being displaced to a larger radius, the fluid possesses a large local angular momentum than its neighbors; therefore, the centrifugal force on the displaced particle, $-\frac{\rho w^2}{r}$ will be greater than the centripetal force, $\frac{\partial p}{\partial r}$ existing at the new location. This particle will tend to move further in same direction (to larger radius) accordingly. As a result, the labilizing effect exists near the outer wall, and the turbulence is promoted. Similarly, there is a stabilizing effect near the inner wall, and this effect will

suppress the turbulence. The hydrodynamic stability described in the curved channel have also been experimentally confirmed in annular pipes in many studies on turbulent swirling flow [7,30,31]. These characteristics of turbulence reflect that the wall shear stress at the outer wall is greater than the wall shear stress at the inner wall. The experimental results show that the wall shear stress at the outer wall is larger, regardless of whether the azimuthal velocity profile of turbulent swirling flow is close to the shape of the free vortex [6, 7, 31] or close to the shape of the forced vortex [30].

In order to represent the difference in the magnitude of the wall shear stresses between the walls, the forced-type vortex, which is the simplest model of swirl, is assumed. Consider the fluid having a solid body rotation (SBR) that rotates around the central axis of the annular pipe. The azimuthal velocity of the fluid is written as

$$w(x, r) = r\omega$$

where r is the radial distance, and ω is the angular velocity.

The angular velocity can be expressed in terms of $\bar{w}$ using the definition of the mean azimuthal velocity.

$$\omega = \frac{\int_{r_i}^{r_o} r dr}{\int_{r_i}^{r_o} r^2 dr} \bar{w} = \frac{3\left(r_o^2 - r_i^2\right)}{2\left(r_o^3 - r_i^3\right)} \bar{w}$$

Let w_o and w_i be the azimuthal velocities near the outer wall and inner wall under the SBR assumption, respectively. Then, these velocities can be written as

$$w_{outer} = r_o\omega = \frac{3r_o\left(r_o^2 - r_i^2\right)}{2\left(r_o^3 - r_i^3\right)}\bar{w}$$
$$w_{inner} = r_i\omega = \frac{3r_i\left(r_o^2 - r_i^2\right)}{2\left(r_o^3 - r_i^3\right)}\bar{w}$$

The total wall shear stresses can then be expressed as follows.

$$\tau_{w_o} = -\frac{f_o}{8}\rho U_{outer}^2$$
$$\tau_{w_i} = \frac{f_i}{8}\rho U_{inner}^2$$

where $U_{outer} = \sqrt{\bar{u}^2 + w_{outer}^2 + \bar{v}^2}$, $U_{inner} = \sqrt{\bar{u}^2 + w_{inner}^2 + \bar{v}^2}$, and f_o and f_i are the Moody friction factor at the outer wall and inner wall, respectively.

$$f_o = \frac{0.316}{\{(1/\zeta)Re_{D_h,outer}\}^{0.25}}$$
$$f_i = \frac{0.316}{\{(1/\zeta)Re_{D_h,inner}\}^{0.25}}$$

where $Re_{D_h,outer} = \frac{\rho U_{outer} 2(r_o - r_i)}{\mu}$ and $Re_{D_{h,},inner} = \frac{\rho U_{inner} 2(r_o - r_i)}{\mu}$.

The tangential wall shear stresses can be computed through the flow angle in the same manner in laminar flows.

$$\tau_{r\theta_o} = \tau_{w_o} \times \frac{w_{outer}}{U_{outer}} \tag{2.11}$$
$$\tau_{r\theta_i} = \tau_{w_i} \times \frac{w_{inner}}{U_{inner}} \tag{2.12}$$

In order to verify equations 2.11 and 2.12, we compare the tangential wall drag between the value from these equations and that from CFD results of section 3.1. The geometry in section 3.1 is selected as the reference geometry

because it is a shape that can see well the effect of wall drag due to no variation of cross-sectional area. For the reasonable comparison, the velocities in the equations 2.11 and 2.12 are obtained from the CFD results.

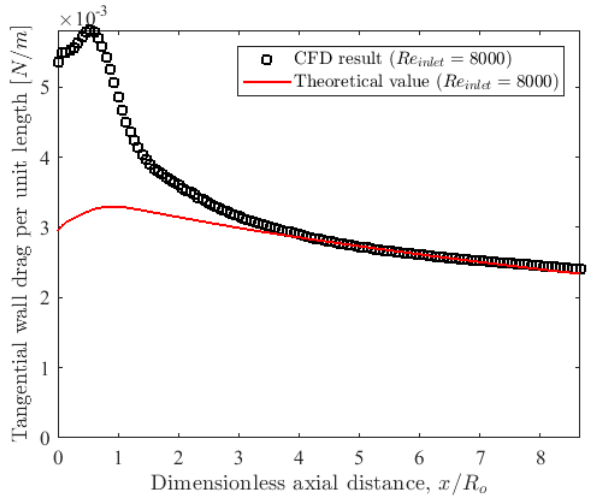

Figure 2.4 The comparison of the tangential wall drag per unit length between the value from the theoretical description and the value from the CFD results.

Figure 2.4 shows the result of the verification. The red solid line is the theoretical tangential wall friction obtained according to the equations 2.11 and 2.12. The black square marker is the tangential wall friction obtained directly from the CFD results. The region of a large discrepancy at the upstream is the transient region which is come from the non-uniformity of the radial direction and the azimuthal direction due to the vane thickness of the swirler. This region where the blockage effect from the vane thickness works, however, is sufficiently short compared to the axial position of the exit of swirl injector, which is the region of interest. In the region where the blockage effect can be ignored, it can be seen that the solid line and the markers are well matched. It can be said that the equations 2.11 and 2.12 are acceptable.

From now on, the tangential wall shear stress in turbulent flow is expressed using the dimensionless variables introduced in section 2.2. The newly introduced variables in a dimensionless form are as follows.

$$\hat{w}_{outer} = \frac{w_{outer}}{\bar{U}_0} = \frac{3\hat{r}_o\left(\hat{r}_o^2 - \gamma^2\right)}{2\left(\hat{r}_o^3 - \gamma^3\right)}\hat{\bar{w}}$$
$$\hat{w}_{inner} = \frac{w_{inner}}{\bar{U}_0} = \frac{3\gamma\left(\hat{r}_o^2 - \gamma^2\right)}{2\left(\hat{r}_o^3 - \gamma^3\right)}\hat{\bar{w}}$$
$$\hat{U}_{outer} = \frac{U_{outer}}{\bar{U}_0}$$
$$\hat{U}_{inner} = \frac{U_{inner}}{\bar{U}_0}$$

where $Re_{inlet} = \frac{\rho\bar{U}_0 2(R_0 - r_i)}{\mu}$ is the inlet Reynolds number, that is, the Reynolds number in the upstream of the swirler.

Then, the wall shear stress terms in equation 2.7 can be expressed as

$$\frac{\tau_{r\theta_o}}{\rho\bar{U}_0^2} = -\frac{f_o\hat{U}_{outer}\hat{w}_{outer}}{8}$$
$$\frac{\tau_{r\theta_i}}{\rho\bar{U}_0^2} = \frac{f_i\hat{U}_{inner}\hat{w}_{inner}}{8}$$

2.4 Verification of model for mean azimuthal velocity using a laminar flow

It is necessary to verify the linear momentum conservation is expressed correctly in the θ direction. Equation 2.4 is solved for laminar flow to obtain $\bar{w}$ and the resulting solution have been compared with CFD results.

For laminar flow, the profile for each velocity component can be expressed analytically. The axial velocity of laminar flow can be expressed with the analytic solution as below:

$$u(x,r) = 2\bar{u}\left[\frac{1-(r/r_o)^2+\frac{1-(r_i/r_o)^2}{\ln(r_o/r_i)}\ln(r/r_o)}{1+(r_i/r_o)^2-\frac{1-(r_i/r_o)^2}{\ln(r_o/r_i)}}\right]$$

The azimuthal velocity can be considered to have a parabolic profile in laminar flow under the concept of fully-developed flow.

$$w(x,r) = -\frac{6\bar{w}}{(r_o-r_i)^2}(r-r_i)(r-r_o)$$

Consider a fixed straight annular pipe ($\alpha = 0$). The radial velocity is therefore considered as zero according to the continuity equation, and $r_o = R_0$. Substitute the expression for wall drag for laminar flow in section 2.3 into equation 2.5, the ODE for $\bar{w}$ can be completed for laminar flow as follows.

$$\begin{aligned} 0 = &-\frac{d}{dx}\int_{r_i}^{r_o}\rho uwrdr + \frac{d}{dx}\left\{\int_{r_i}^{r_o} r\mu\frac{dw}{dx}dr\right\} \\ &+\int_{r_i}^{r_o}\mu\left(\frac{\partial w}{\partial r}-\frac{w}{r}\right)dr - \frac{4\zeta\mu\,(r_o+r_i)}{(r_o-r_i)}\bar{w} \end{aligned} \tag{2.13}$$

where ζ is the correction factor described in section 2.3 and $r_o = R_0$ due to $\alpha = 0$ in this case.

Equation 2.13 is linear second-order ODE for the mean azimuthal velocity, and it can be solved analytically. However, since the solution is very complicated, it is omitted in the paper.

The computational domain of CFD simulation used for the verification is represented in figure 2.5.

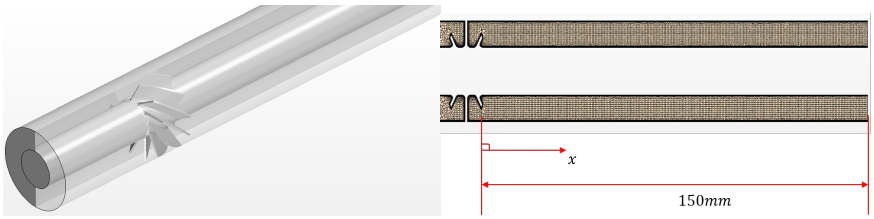

Figure 2.5 Computation domain of CFD for laminar swirling flow.

A flat-vane axial swirler with a vane angle of 40 degrees is used as the swirl generator. A straight annular pipe with an outer radius of 15 mm, and an inner radius of 7 mm is used.

The result of the comparison of equation 2.13 and CFD results is shown in figure 2.6. The initial value, $\bar{w}(0)$, is required to plot the solution obtained in equation 2.13. This value is obtained from the CFD results.

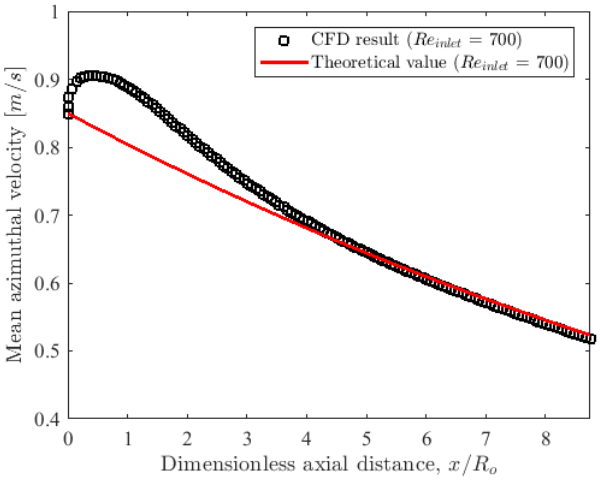

Figure 2.6 Verification of linear momentum conservation.

Figure 2.6 shows that the mean azimuthal velocity obtained from equation 2.13 agrees well with the result of the detailed numerical simulation. The region

which shows inconsistency ($0 < x/R_0 < 4.5$) is the transient region where the effect of swirler vane thickness exists. From the region where this blockage effect vanishes ($x/R_0 > 4.5$), the rate of change of $\bar{w}$ from equation 2.13 agrees well with the CFD results. Thus, it can be confirmed that the linear momentum conservation described through RTT is well described.

2.5 Description of the eddy viscosity

In turbulent flow, which is a flow regime of interest in the study, the effective viscosity differs from the molecular viscosity due to the presence of turbulence. The effective viscosities in the ODE for $\bar{w}$ is expressed as the summation of the molecular viscosity and the eddy viscosity for turbulent flow.

$$\mu_{r\theta}^{eff} = \mu + \rho\epsilon_{r\theta}$$
$$\mu_{x\theta}^{eff} = \mu + \rho\epsilon_{x\theta}$$

where $\epsilon_{r\theta} = -\overline{v'w'}$ and $\epsilon_{x\theta} = -\overline{u'w'}$. u', w', and v' are the turbulent velocities in the x, θ, and r directions, respectively.

A model for eddy viscosity is needed, for an eddy viscosity dominates a molecular viscosity in most flow regions. There are a number of models for eddy viscosity, that is turbulence models. A simple and reliable model should be used for the simplicity of the one-dimensional model for the swirl decay rate. There are two candidates: (1) a mixing length model and (2) Reichardt's correlation of eddy viscosity. In addition, turbulence is highly anisotropic in the case of swirling flow [18, 21], so it is more accurate to distinguish the direction of eddy viscosity. However, in this study, the direction of turbulence is not considered for the simplicity of the numerical model. That is,

$$\epsilon_{r\theta} = \epsilon_{x\theta} = \epsilon$$

The effective viscosities are then written as

$$\mu_{r\theta}^{eff} = \mu_{x\theta}^{eff} = \mu_{eff} = \mu + \rho\epsilon$$

Mixing length model Mixing length model is the simplest and earliest models for eddy viscosity. This model uses the concept of mixing length, which is the length scale of turbulence where a velocity gradient respect to the positions can be regarded as linear. According to this model, eddy viscosity can be expressed as

$$\epsilon = l_m^2 \left| \frac{\partial V}{\partial r} \right|$$

where l_m is the mixing length, and $V = \sqrt{u^2 + w^2 + v^2}$ is the (time-averaged) bulk velocity.

The mixing length in tube can be expressed according to Nikuradse's empirical relationship as

$$l_m = \frac{r_o - r_m}{50} \left(1 - \left(\frac{r - r_m}{r_o - r_m} \right)^2 \right) \left(7 + 3 \left(\frac{r - r_m}{r_o - r_m} \right)^2 \right)$$

where r_m is the radial position with the maximum velocity and is considered to be the middle point between the inner and outer walls, $r_m = \frac{r_i + r_o}{2}$.

For the bulk velocity, V, the distribution to the r direction must be considered. One-seventh law, which is generally used as the mean velocity profile of internal turbulent flow, can be applied. For the annular pipe, there are two walls, outer and inner walls, so the flow region can be divided into the outer

region, $r > r_m$ and inner region, $r < r_m$. Then, the profile of V can be written as follows.

$$V_{inner} = V_{max}\left(\frac{2r + 2r_i}{r_o + r_i}\right)^{1/7}$$
$$V_{outer} = V_{max}\left(\frac{2r_o - 2r}{r_o + r_i}\right)^{1/7}$$

where V_{max} is the maximum value of V and is assumed as $\bar{U} = \sqrt{\bar{u}^2 + \bar{w}^2 + \bar{v}^2}$. Therefore, the eddy viscosity from mixing length model is expressed as

$$\epsilon = \begin{cases} \left(\frac{r_i - r_o}{100}\right)^2 \left(\frac{r_i - 2r + r_o}{(r_i - r_o)^2} - 1\right)^2 \left(\frac{3(r_i - 2r + r_o)}{(r_i - r_o)^2} + 7\right)^2 \sqrt{\frac{4\bar{U}^2}{49\left(\frac{2r + r_i}{r_i + r_o}\right)^{12/7}(r_i + r_o)^2}} \\ \left(r_i < r < (r_i + r_o)/2\right) \\ \\ \left(\frac{r_i - r_o}{100}\right)^2 \left(\frac{r_i - 2r + r_o}{(r_i - r_o)^2} - 1\right)^2 \left(\frac{3(r_i - 2r + r_o)}{(r_i - r_o)^2} + 7\right)^2 \sqrt{\frac{4\bar{U}^2}{49\left(-\frac{2r - r_o}{r_i + r_o}\right)^{12/7}(r_i + r_o)^2}} \\ \left((r_i + r_o)/2 < r < r_o\right) \end{cases} \tag{2.14}$$

Reichardt's eddy viscosity model In 1951, Reichardt [28] proposed a expression for eddy viscosity from experimental measurements on turbulent flow in a circular pipe. Michiyoshi [26] applied the equation of Reichardt to the annular pipe and proposed the equation for eddy viscosity as follows.

$$\epsilon = \begin{cases} \frac{U_o^*(r_o - r_m)}{15}\left(1 - \left(\frac{r_m - r}{r_m - r_i}\right)^2\right)\left(1 + 2\left(\frac{r_m - r}{r_m - r_i}\right)^2\right)\left[1 - \left(1 - \frac{S^*}{\sqrt{\tau^*}}\right)\frac{r_m - r}{r_m - r_i}\right] \\ (r_i < r < r_m) \\ \\ \frac{U_o^*(r_o - r_m)}{15}\left(1 - \left(\frac{r - r_m}{r_o - r_m}\right)^2\right)\left(1 + 2\left(\frac{r - r_m}{r_o - r_m}\right)^2\right) \\ (r_m < r < r_o) \end{cases} \tag{2.15}$$

where $U_o^* = \sqrt{\frac{\tau_{w_o}}{\rho}}$ is the friction velocity at the outer wall, r_m is the radial position with the maximum velocity, $S^* = \frac{r_m - r_i}{r_o - r_m}$ is the dimensionless parameter, and $\tau^* = \frac{\tau_{w_o}}{\tau_{w_i}}$ is the wall shear stress ratio.

Let $r_m = \frac{r_o + r_i}{2}$. Also, for simplicity, the difference between the wall shear stresses at the outer and inner wall is not considered, unlike the discussion in section 2.3. This is also because, according to equation 2.15, r_m will be a discontinuous point. Instead, the wall shear stress is simply calculated without the assumption of SBR in section 2.3 as follows.

$$f_m = \frac{0.316}{\left((1/\zeta)\, Re_{D_h}\right)^{0.25}}$$
$$Re_{D_h} = \frac{\rho \bar{U} 2(r_o - r_i)}{\mu}$$
$$\tau_{w_m} = \frac{f_m}{8}\rho \bar{U}^2$$

where τ_{w_m} is the wall shear stress without the SBR assumption in section 2.3, and $\bar{U} = \sqrt{\bar{u}^2 + \bar{w}^2 + \bar{v}^2}$ is the total velocity. Then, equation 2.15 can be rewritten as

$$\epsilon = \frac{U^*\left(r_o - r_i\right)}{30}\left(1 - \left(\frac{2r - r_o - r_i}{r_o - r_i}\right)^2\right)\left(1 + 2\left(\frac{2r - r_o - r_i}{r_o - r_i}\right)^2\right) \quad (2.16)$$

where $U^* = \sqrt{\frac{\tau_{w_m}}{\rho}}$ is the friction velocity.

Comparison between the models for eddy viscosity descriptions A comparison with the CFD result for inlet Reynolds number of 8,000 in section 3.1 is shown in figure 2.7. The velocity values required to described equation 2.14 and 2.16 were obtained from the CFD results. All data in figure 2.7 are values at $x/R_0 = 5$ position where the blockage effect induced from the vane thickness vanishes.

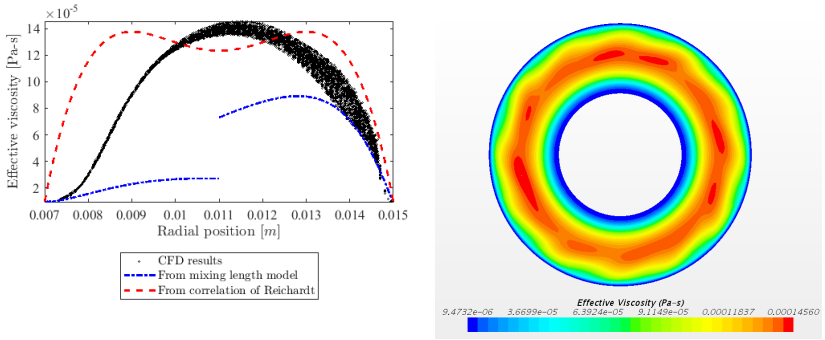

Figure 2.7 Comparison of the models for eddy viscosity description and contour of effective viscosity at $x/R_o = 5$ from CFD.

Figure 2.7 shows that the eddy viscosity obtained from the mixing length model is significantly different from the CFD results in all regions. Equation 2.16, obtained from Reichardt's correlation, deviates from the CFD results in the region near the inner wall ($7\,mm < r < 8.8\,mm$). However, it shows acceptable values in other regions. From the comparison in figure 2.7, it can be seen that equation 2.16 is more appropriate than equation 2.14.

Using equation 2.16, the effective viscosity can be expressed with the dimensionless variables introduced in section 2.2 as

$$\mu_{eff} = \mu\left(1+\Psi\right)$$

where $\Psi = \frac{Re_{inlet}(\hat{r}_o-\gamma)}{60(1-\gamma)}\sqrt{\frac{f_m}{8}\hat{\bar{U}}^2}\left(1-\left(\frac{2\hat{r}-\hat{r}_o-\gamma}{\hat{r}_o-\gamma}\right)^2\right)\left(1+2\left(\frac{2\hat{r}-\hat{r}_o-\gamma}{\hat{r}_o-\gamma}\right)^2\right)$, and $Re_{inlet} = \frac{\rho\bar{U}_0 2(R_0-r_i)}{\mu}$ is the inlet Reynolds number, that is, the Reynolds number in the upstream of the swirler.

2.6 A new model for swirl number in turbulent flows

From the discussion so far, equation 2.7 can be written as

$$\begin{aligned}0 = &-\frac{d}{d\hat{x}}\int_\gamma^{\hat{r}_o}\hat{\bar{u}}\hat{\bar{w}}\hat{r}d\hat{r} - \int_\gamma^{\hat{r}_o}\hat{v}\hat{\bar{w}}d\hat{r} + \frac{2\left(1-\gamma\right)}{Re_{inlet}}\frac{d}{d\hat{x}}\left\{\frac{d\hat{\bar{w}}}{d\hat{x}}\int_\gamma^{\hat{r}_o}\left(1+\Psi\right)\hat{r}d\hat{r}\right\}\\ &-\frac{2\left(1-\gamma\right)\hat{\bar{w}}}{Re_{inlet}}\int_\gamma^{\hat{r}_o}\frac{1+\Psi}{\hat{r}}d\hat{r} + \left(\frac{\tau_{r\theta_o}}{\rho U_0^2}\right)\frac{\hat{r}_o}{\cos\alpha} - \left(\frac{\tau_{r\theta_i}}{\rho U_0^2}\right)\gamma \qquad (2.17)\end{aligned}$$

where

$$\Psi = \frac{Re_{inlet}\left(\hat{r}_o-\gamma\right)}{60\left(1-\gamma\right)}\sqrt{\frac{f_m}{8}\hat{\bar{U}}^2}\left(1-\left(\frac{2\hat{r}-\hat{r}_o-\gamma}{\hat{r}_o-\gamma}\right)^2\right)\left(1+2\left(\frac{2\hat{r}-\hat{r}_o-\gamma}{\hat{r}_o-\gamma}\right)^2\right)$$

$$\frac{\tau_{r\theta_o}}{\rho U_0^2} = -\frac{f_o\hat{U}_{outer}\hat{w}_{outer}}{8}$$

$$\frac{\tau_{r\theta_i}}{\rho U_0^2} = \frac{f_i\hat{U}_{inner}\hat{w}_{outer}}{8}$$

The decay rate of swirl is then

$$\frac{S}{S_0} = \frac{\hat{r}_o^3-\gamma^3}{\hat{r}_o\left(1-\gamma^3\right)}\left(\frac{\hat{\bar{w}}}{\hat{\bar{w}}_0}\right) \qquad (2.18)$$

where S is the swirl number at the some axial position, x, and the subscript 0 means the value at the reference position, $x = 0$ that is the region close to the swirler exit.

S_0 can be obtained from commonly used correlations such as the correlation of Beer and Chigier for flat-vane axial swirler [2] or the correlation of Sheen et al. for radial-type swirler [32]. By combining these equations with equation 2.18, the swirl number, $S(x)$ can be fully-described.

Equation 2.17 should be solved numerically because there is no analytic solution. Mathematically, this ODE is a two-points boundary value problem with boundary conditions at $\hat{x} = 0$ and $\hat{x} \to \infty$. The boundary condition at $\hat{x} \to \infty$ can be considered as zero. The mean azimuthal velocity at the swirler exit, $\bar{w}_0$ can be obtained through various methods. There might be a way to compute $\bar{w}_0$ using an existing correlation for swirl number that gives somewhat reliable value at the swirler exit. For example, from the correlation of Beer and Chigier, the swirl number close to the flat-vane axial swirler can be written as

$$S_0 \simeq \frac{2}{3}\left(\frac{1-\gamma^3}{1-\gamma^2}\right)\tan\phi$$

S_0 can be also written from the definition of the swirl number as below.

$$S_0 = \frac{\int_{r_i}^{R_0} \rho u_0 w_0 r^2 dr}{R_0 \int_{r_i}^{R_0} \rho u_0^2 r dr} \simeq \frac{2}{3}\left(\frac{1-\gamma^3}{1-\gamma^2}\right)\left(\frac{\bar{w}_0}{\bar{U}_0}\right)$$

Therefore, $\bar{w}_0$ can be simply estimated for a flat-vane axial swirler in the following manner.

$$\hat{\bar{w}}_0 = \frac{\bar{w}_0}{\bar{U}_0} \simeq \left(\frac{1}{1-\sigma}\right)\tan\phi \tag{2.19}$$

where ϕ is a vane angle of swirler as shown in figure 3.2, and σ is the blockage ratio. $\left(\frac{1}{1-\sigma}\right)$ is multiplied because the azimuthal velocity at $x = 0$ is actually

generated as the flow passes through the narrowed cross-section according to the blockage ratio.

The blockage ratio, σ can be defined as the ratio which is between the axially blocked area by the vane thickness of the swirler and the cross-sectional area of the annular pipe at the location where the swirler is located.

$$\sigma = \frac{A_{block}}{A_0}$$

As discussed previously and the results of CFD show, a very complicated flow occurs due to the azimuthal and radial non-uniformity generated by the vane thickness near the swirler exit, and thus the transient region deviating from the trend of the swirl decay exists. Equation 2.18 is intended to predict the swirl number at the swirl injector exit, so this complex flow region, which is mush shorter than the exit distance of the swirl injector, is not covered in the derivation. Therefore, equation 2.18 does not predict the swirl number variation in the transient region, and this can cause some problems in predicting the swirl number at the swirl injector exit. This problem can be solved by correcting for boundary condition at $\hat{x} = 0$. The correction can be done by multiplying the value in equation 2.19 by $\left(\frac{1}{1-\sigma}\right)$ again as in equation 2.20.

$$\left(\hat{\tilde{w}}_0\right)_{bd} = \left(\frac{1}{1-\sigma}\right)^2 \tan\phi \tag{2.20}$$

This correction converts the $\hat{\tilde{w}}_0$ to that value when the vane thickness is infinitely thin, $\left(\hat{\tilde{w}}_0\right)_{bc}$. By using the value in equation 2.20, the swirl number can be predicted more accurately by the proposed one-dimensional numerical model.

The blockage ratio, σ can be approximated for a flat-vane axial swirler as follows.

$$\sigma \simeq \left(\frac{ztH}{\cos\theta}\right) \times \frac{1}{A_0} = \frac{ztH}{\pi\left(R_0^2 - r_i^2\right)\cos\phi}$$

where z is the number of vanes, t is the thickness of vanes, H is the height of vane, and ϕ is the vane angle of swirler.

Chapter 3

Validation of the proposed model for the swirl number

In this chapter, equation 2.18 will be validated. The validity of the newly proposed one-dimensional numerical model will be determined through comparison with CFD results. The turbulence model used in all validation cases is a Reynolds stress model (RSM) or k-ω SST turbulence. Previous studies have shown that RSM [18, 19] and k-ω SST turbulence [9] show acceptable results in simulation of swirling flow. Since the velocity profile of the swirl near the wall is known to deviate significantly from the logarithmic law [18, 21], all simulations for validation is calculated with a low-$y+$ wall treatment using a fine mesh ($y+ \sim 1$) near the wall to avoid standard wall function.

$\hat{\bar{w}}_0$ is required to numerically solve equation 2.17 as described in section 2.6. In this chapter, $\bar{w}_0$ from the each CFD result is used for more fair comparison about the decay rate of swirl. This value, however, is corrected using the concept of blockage ratio as described in section 2.6, and the corrected value is used as the boundary condition, $\left(\hat{\bar{w}}_0\right)_{bd}$.

$$\left(\hat{\hat{w}}_0\right)_{bd} = \left(\frac{1}{1-\sigma}\right)\hat{\hat{w}}_{0,CFD}$$

3.1 Validation in a straight coannular swirl injector

In this section, the swirl injector, which is a straight annular pipe with $\gamma = \frac{7\,mm}{15\,mm}$ as shown in figure 3.1, is considered.

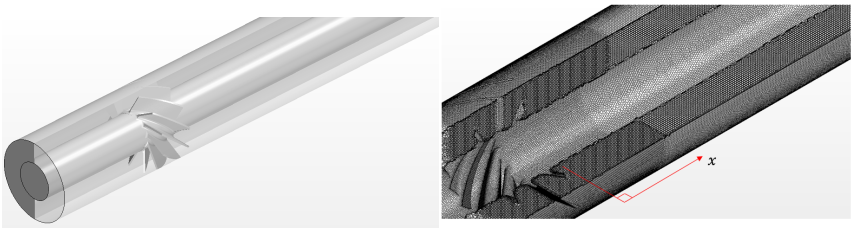

Figure 3.1 Computational domain of section 3.1.

The swirl generator in this geometry is a flat-vane axial swirler with a vane angle of 40 degrees as shown in figure 3.2. The blockage ratio of this swirl generator is about 0.14.

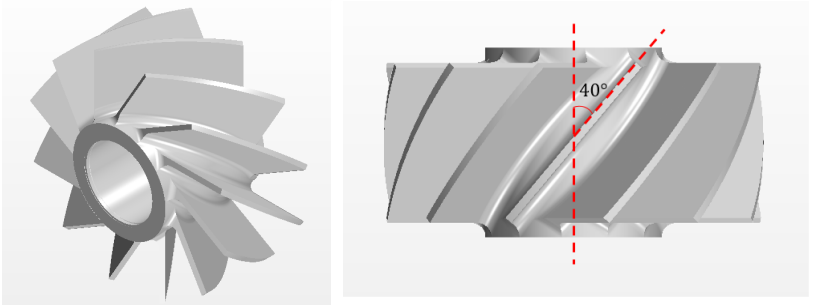

Figure 3.2 A flat-vane axial swirler with 40 degrees vane angle.

For this geometry, CFD simulations for validation were performed with inlet Reynolds number of 8,000 and 12,000 using RSM of turbulence. A grid test was

conducted to minimize the numerical error. The calculation was performed for the three-types of meshes shown in table 3.1.

Type	Mesh 1	Mesh 2	Mesh 3
Number of cells	1,050,228	3,693,109	5,823,627

Table 3.1 Property of different grid.

The test results for $Re_{inlet} = 8,000$ case are shown in figure 2.18. Figure 3.3 shows that mesh 2 and mesh 3 have the same results. Since mesh 2 has fewer grids, this grid is selected for computational efficiency.

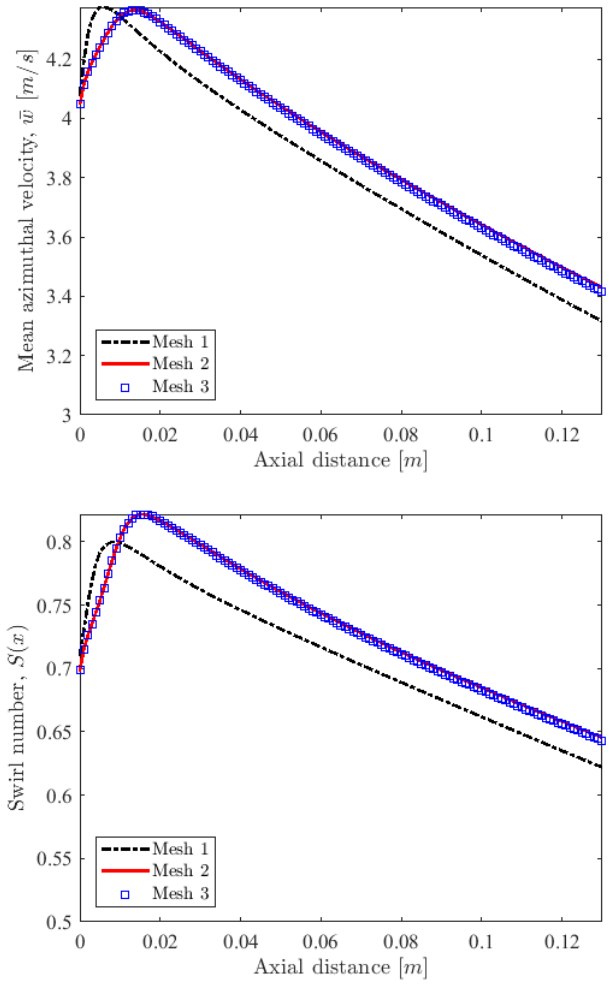

Figure 3.3 Grid test results.

The validation results are shown in figure 3.4. This figure shows the swirl number from the proposed model is in good agreement with the CFD results in both cases, $Re_{inlet} = 8,000$ and $Re_{inlet} = 12,000$. It is notable that the case of $Re_{inlet} = 12,000$ shows the swirl decay rate is slightly smaller than that of the case of $Re_{inlet} = 8,000$. This phenomena will be covered in detailed in chapter 4.

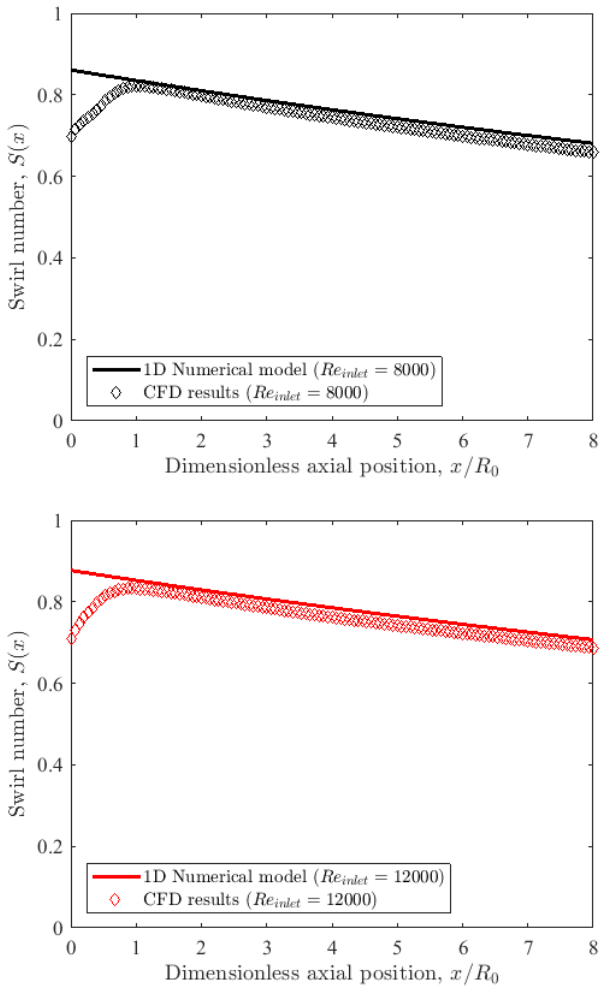

Figure 3.4 Validation results in section 3.1.

3.2 Validation in a coannular swirl injector with variable cross-sectional area

The computational domain for this section is shown in figure 3.5. It is a swirl injecting pipe with a variable cross-sectional area of $\tan^{-1}(1/20)$ and $\gamma = \frac{7\,mm}{15\,mm}$. The CFD simulations were conducted for two inlet Reynolds number of

8,000 and 12,000. The flat-vane axial swirler shown in figure 3.2 was used as the swirl generator in both cases. The turbulence model used in the simulations is RSM of turbulence as in section 3.1.

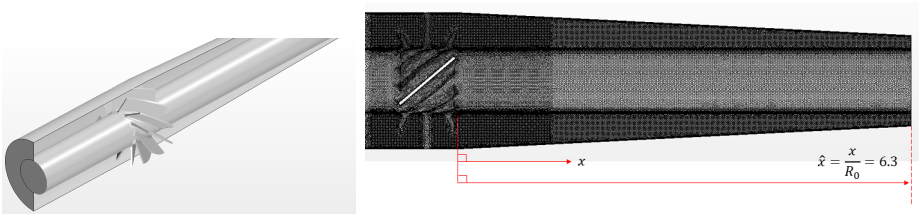

Figure 3.5 Computational domain of section 3.2.

The comparison result is shown in figure 3.6. Figure 3.6 also show that the proposed equation well reflects the swirl decay rate and as a result predicts the swirl number well at the exit of the swirl injector. In this geometry, the swirl decay rate is much larger in all cases than that of the swirl injector in section 3.1. Therefore. if there is a change in cross-sectional area, a more careful analysis of the selection of swirler or swirl injector will be needed to obtain the desired swirl number at the end of the swirl injector. It is expected that the proposed model of variation of swirl number is very useful for the selection of appropriate swirler to obtain the desired swirl number in this type of swirl injectors. This usefulness of the proposed model is discussed in detial in section 4.1. It can be also seen that the difference between the different inlet Reynolds numbers is smaller than the result from the section 3.1. It seems that the effect of the change in cross-sectional area on swirl decay rate is more dominant than the effect of Re_{inlet} on the decay rate of swirl.

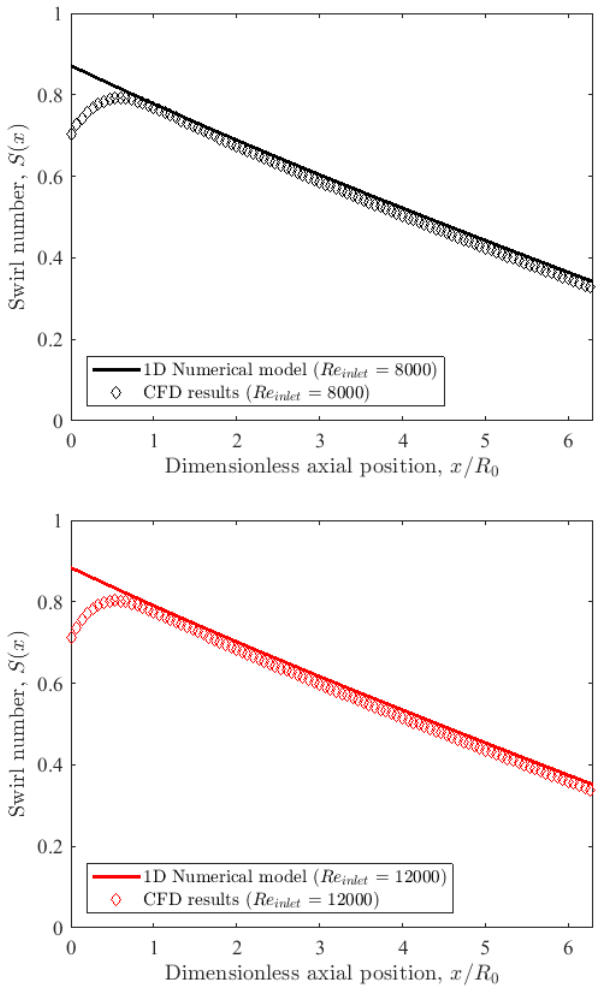

Figure 3.6 Validation results in section 3.2.

3.3 Validation in a coannular swirl injector connected to a swirl-stabilized burner

In this case, the geometry is the shape of the swirl injector connected to the actual swirl-stabilized burner. In this case, the swirl generators used in the simulations are a flat-vane axial swirler with a vane angle of 40 degrees in

figure 3.2, as well as a flat-vane axial swirler with a vane angle of 70 degrees such as figure 3.7. The blockage ratio of the swirler having a vane angle of 70 degrees is 0.19.The shape of the swirl injecting pipe is a converging annular pipe with $\gamma = \frac{7\,mm}{15\,mm}$ and a converging angle, $\alpha = \tan^{-1}(5/54)$ as shown in figure 3.8. The turbulence model used in the CFD simulations is k-ω SST of turbulence. The validation is performed on the flow with inlet Reynolds number of 3,000.

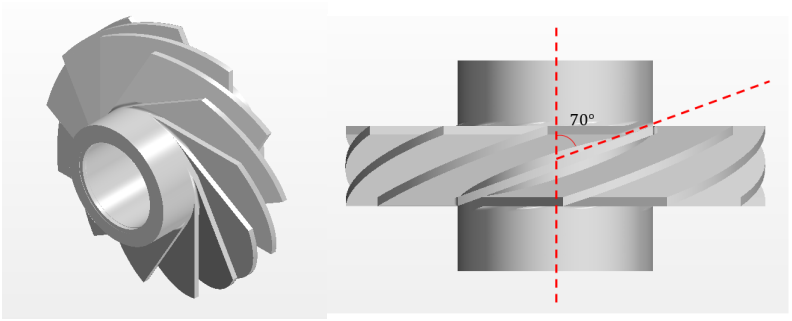

Figure 3.7 A flat-vane axial swirler with 70 degrees vane angle.

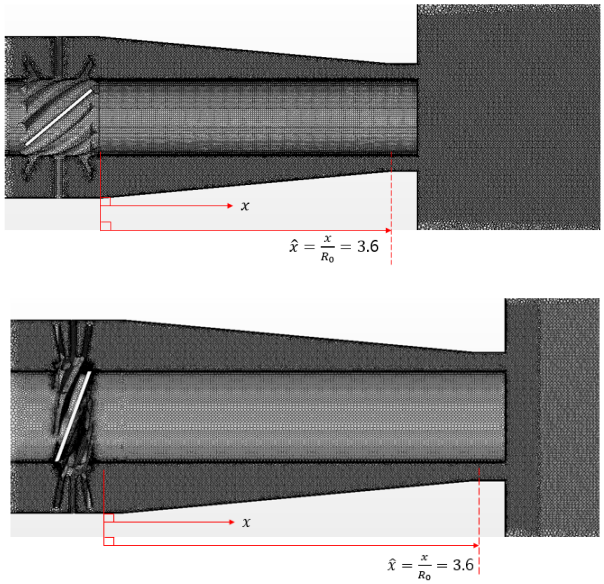

Figure 3.8 Computational domain of section 3.3:(top) the case using a flat-vane axial swirler with vane angle of 40 degree; and (bottom) the case using a flat-vane axial swirler with vane angle of 70 degree.

The comparison results are shown in figure 3.9. The proposed model also shows good agreement with the CFD results. Figure 3.9 implies that the swirl decay rate varies with the initial swirl intensity. That is, the larger the initial swirl intensity, the greater the swirl decay rate. This is consistent with previous experimental studies [3, 6]. This will be covered in section 4.4.

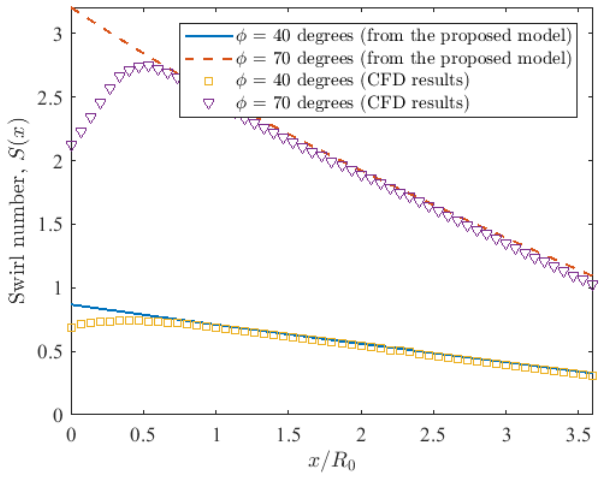

Figure 3.9 Validation results in section 3.3.

Chapter 4

Application of a new model

4.1 Selection of the proper swirler in a swirl-stabilized burner to produce the desired flow

As can be seen in chapter 3, the swirl number varies considerably, especially in swirl injecting pipes where the cross-sectional area changes. Therefore, it is difficult to select the appropriate swirler for the desired swirl number in this type of swirl injector by using the existing correlation that cannot express the swirl decay. Even if a relatively simple Reynolds-averaged Navier-Stokes (RANS) simulation is conducted, it would be difficult to simulate all of the candidate swirlers, because a lot of calculations are necessary for proper calculation as can be seen in the grid test in chapter 3. However, in the case of the proposed one-dimensional model, it is extremely simple to obtain the swirl numbers in swirl injecting pipes.

Suppose there is a swirl injector with $\gamma = 7\,mm/15\,mm$ and a converging angle of $\tan^{-1}(5/54)$ as shown in figure 4.1. The proposed model can easily

answer which swirler should be used to have a specific swirl number at the burner inlet. According to Chigier [4], the swirl number at the burner inlet should be larger than 0.6 in order to obtain a sufficient size of CTRZ. Suppose that the four flat-vane axial swirlers listed in table 4.1 are available as a swirl generator in the swirl-stabilized burner.

	Swirler 1	Swirler 2	Swirler 3	Swirler 4
Vane angle, ϕ	40 degrees	50 degrees	60 degrees	70 degrees
Blockage ratio, σ	0.14	0.17	0.20	0.19

Table 4.1 Available flat-vane axial swirler in swirl-stabilized burner.

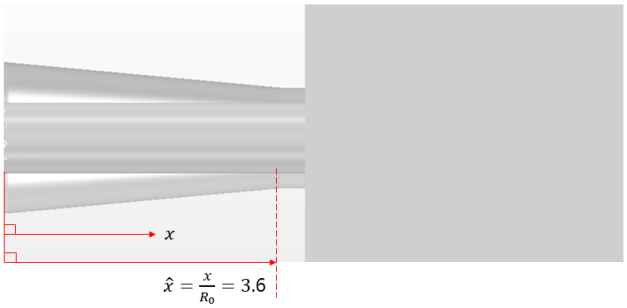

Figure 4.1 A swirl injector connected to a swirl-stabilized burner.

Suppose the inlet Reynolds number is 3,000. From the proposed model, the variations of the swirl number in the swirl injector when each swirler is used can be computed. In these computation, the boundary condition, $\left(\hat{\bar{w}}_0\right)_{bd}$ is obtained by using the equation of Beer and Chigier, which are the correlation of S_0 described in section 2.6. That is,

$$\left(\hat{\bar{w}}_0\right)_{bd} = \left(\frac{1}{1-\sigma}\right)^2 \tan\phi$$

Then, the swirl number, $S(x)$ can be written from equation 2.18 as

$$S = \frac{2}{3}\left\{\frac{\hat{r}_0^3 - \gamma^3}{\hat{r}_0\left(1-\gamma^2\right)}\right\}\hat{\bar{w}}$$

The result is shown in figure 4.2. As can be seen in figure 4.2, Swirler 3 or 4 should be used to achieve the desired swirl number, $S_c = 0.6$. In other words, through the proposed model, it can be seen that a swirl-stabilized burner using the swirl injector shown in figure 4.1 would be able to generate CTRZ properly only by using swirler 3 or 4 under the inlet Reynolds number 3,000 condition.

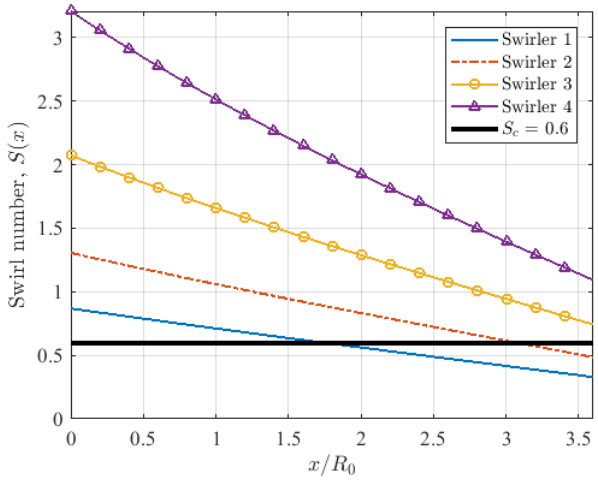

Figure 4.2 Variation of swirl number in swirl injector from the proposed model when each swirler is used.

CFD simulations were performed using k-ω SST turbulence model for each case to see the flow fields when using each swirler. The results of CFD simulations for each case are shown in figure 4.3. From figure 4.3, it can be seen that CTRZ is not formed properly in the cases of swirler 1 and 2, but a sufficient size of CTRZ is gradually formed in the case of swirler 3 and very large CTRZ is formed in the case of swirler 4 as expected from the figure 4.2.

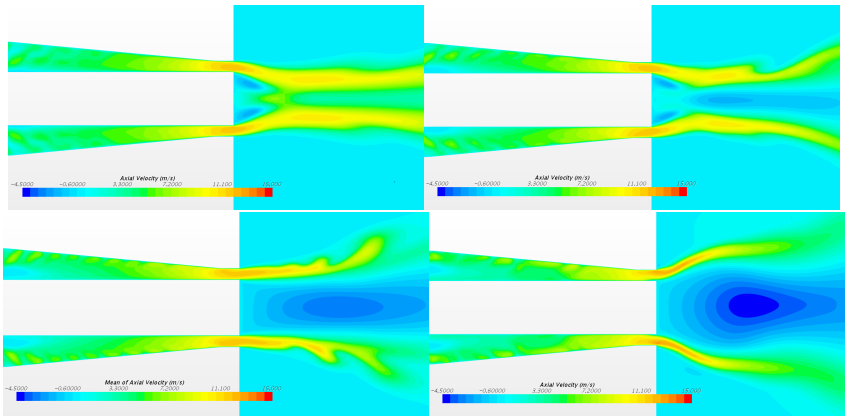

Figure 4.3 Contours of axial velocity in swirl-stabilized burner: (top left) the case of swirler 1; (top right) the case of swirler 2; (bottom left) the case of swirler 3; and (bottom right) the case of swirler 4.

The proposed model shows the swirl number change in swirl injecting pipe without excessive calculation. If the particular swirl injecting pipe to be used in the swirl-stabilized burner, the proposed model can be used to determine which swirlers should be used to produce the desired type of flow in the burner. Conversely, if the swirler is determined, then the proposed model will also give an answer on which swirl injecting pipe should be used to obtain the desired swirl number.

4.2 Variation of swirl decay rate with the ratio of the inner radius to the outer radius in swirl injectors

The proposed one-dimensional model for decay of swirl, Equation 2.18 is a function of Re_{inlet}, γ, $\hat{x}$, and α, so we can see how the swirl decay rate changes according to $\gamma = r_i/R_0$. Figure 4.4 shows the change in decay of swirl when γ is varied from 0.01 to 0.99 in a straight annular pipe with an inlet Reynolds

number of 12,000 and $\left(\hat{\bar{w}}_0\right)_{bd} = 1$. From the figure, it can be seen that the swirl decay rate decreases as γ increases from 0.01 to 0.4, and the values above, the swirl decay rate increases as γ increases. This fact is consistent with the experimental results of Clayton et al. [6]. Their experiment showed that the swirl decay rate at $\gamma = 0.61$ is greater than at $\gamma = 0.51$. Figure 4.4 implies that there is a γ that minimizes the swirl decay rate in a straight annular pipe.

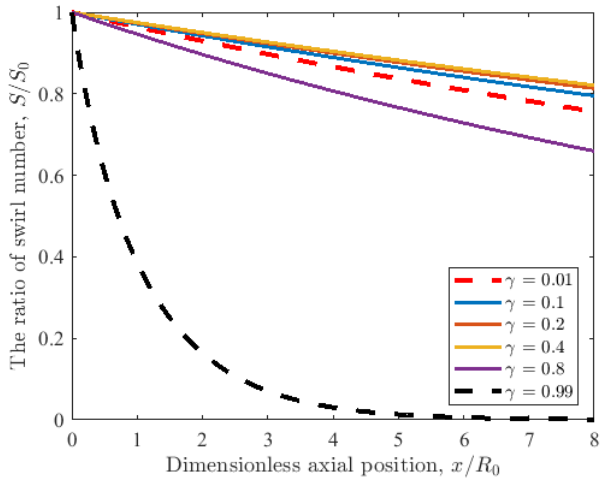

Figure 4.4 Variation of decay rate of swirl with $\gamma = r_i/R_0$.

Therefore, for more detail, the swirl decay rate was calculated while changing γ from 0.3 to 0.55 at intervals of 0.5, which is shown in figure 4.5. Figure 4.5 shows that when $\gamma \sim 0.35$ the swirl decay rate in a straight annular pipe can be minimized. From this result, it seems that the swirl decay rate can be minimized in a straight annular pipe with γ of about 0.35, if all other conditions are the same.

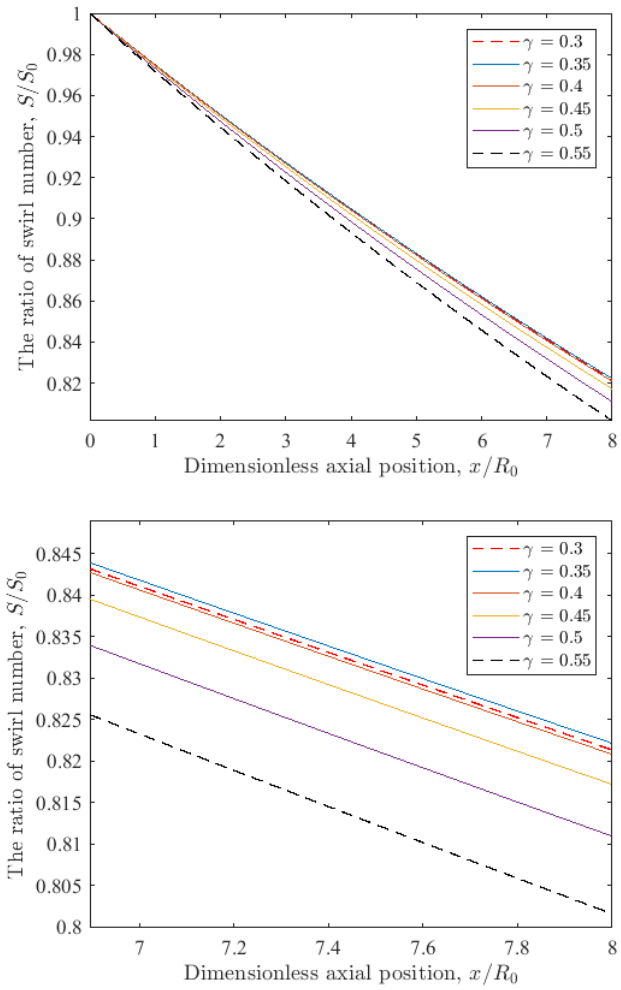

Figure 4.5 Swirl decay rate when γ is varied from 0.3 to 0.55.

4.3 Variation of swirl decay rate with inlet Reynolds number

In this time, it is examined that how the swirl decay rate changes by varying Re_{inlet} in a straight annular pipe with $\gamma = 0.4$ from equation 2.18. The results are shown in figure 4.6.

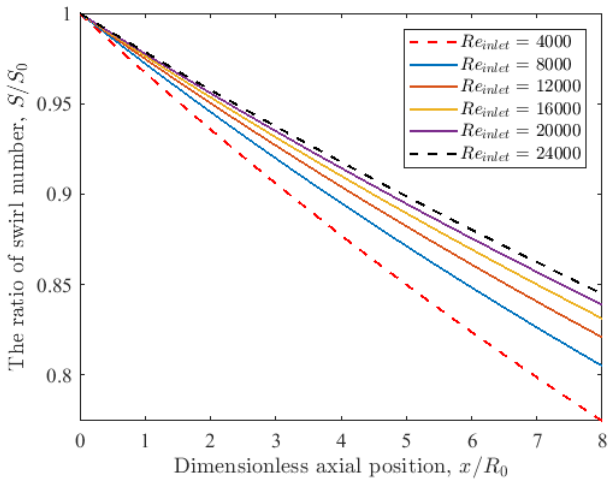

Figure 4.6 Swirl decay rate when when Re_{inlet} is varied from 4,000 to 24,000.

Figure 4.6 shows that as the inlet Reynolds number increases, the swirl decay rate decreases. These results are consistent with the results of previous studies [13, 22, 40].

4.4 Variation of swirl decay rate with the initial swirl intensity

Equation 2.17 is two-points boundary value problem and implies that the decay rate of swirl can vary according to the initial swirl intensity, or $\hat{\bar{w}}_0$. Therefore, an analysis of how the swirl intensity varies while changing $\hat{\bar{w}}_0$, that is, changing the initial swirl intensity, S_0, was performed through the proposed model. Consider a straight annular pipe with $\gamma = 0.4$. The inlet Reynolds number is considered as $5,000$, and the blockage ratio is considered as zero. The result is shown in figure 4.7.

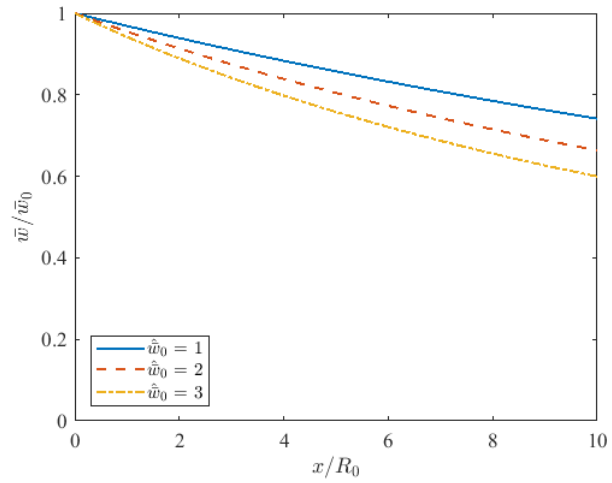

Figure 4.7 Variation of decay rate of swirl with initial swirl intensity.

Figure 4.7 shows that the larger the initial swirl intensity, the greater decay rate of swirl. This fact also can be seen in figure 4.2. These results show the same phenomenon as other experimental studies [3, 6].

Chapter 5

Conclusion

The primary objective of this study is to model the decay rate of swirl to estimate the swirl number in a swirl injector. Especially, in the swirl injecting pipe with the change of the cross-sectional area, the existing correlation of swirl number does not reflect the tendency of the swirl number variation. Since the swirl number at the burner inlet is one of the important factors that determine the flow characteristics in swirl-stabilized burner, it is important to predict the swirl number change in the swirl injector for the design of appropriate swirl-stabilized burner. Therefore, it is mainly aimed to predict the swirl number change in swirl injectors.

A new one-dimensional model to predict the swirl decay rate is proposed to estimate the swirl intensity at the end of the swirl injector in this study. The linear momentum conservation in the tangential direction is described with RTT and this conservation equation is used for the derivation. The main factor in the change of angular momentum of swirl is the wall drag. Therefore, the Moody friction factor is used to describe the wall shear stress by using the existing

formulas. Because the existing formulas for Moody friction factor is applicable to the circular pipe, these formulas are corrected to be applicable to the annular pipe. The tangential wall shear stress is described through the assumption of the direction of the wall drag, and it was found to be in good agreement with the CFD results. To verify that the linear momentum conservation expressed through RTT is properly described, the verification is carried out by comparison with CFD results in laminar flow. As a result, it can be confirmed that the ODE is properly described. For turbulent flow, eddy viscosity has to be considered. Although anisotropy of turbulence is significant in swirling flow, the direction of turbulence is not considered for simple modeling. The empirical correlation of Reichardt and mixing length model are used to describe the eddy viscosity. Compared with CFD results, Reichardt's correlation is more acceptable than the mixing length model. To determine the validity of the proposed model, the comparison with the results of CFD simulations is carried out in various shapes of swirl injectors. The newly proposed model well predicts the variation of the swirl number in the swirl injecting pipe for all cases.

Through the proposed model, it was investigated how the decay rate of swirl varies by changing various factors which are considered to affect the swirl decay rate. The change in the swirl decay rate is observed as the inlet Reynolds number, γ, and initial swirl intensity are changed. The proposed model showed that the swirl decay rate decreases as inlet Reynolds number increases and initial swirl intensity decreases. This is consistent with previous experimental results. It has also been shown that a straight annular pipe can minimize the decay of swirl when having a specific γ. This value is estimated about 0.35.

There is a non-uniformity in azimuthal and radial directions in a near region of swirler exit due to the area of swirler. The flow in this transient region is very complicated and deviates much from the tendency of swirl decay. However, in

the swirl injecting pipe, this region is limited to a very restricted portion. Since the main purpose of the proposed model is to predict the swirl number at the end of the swirl injector, the detailed analysis is not performed for this region in this study. Instead, the concept of blockage ratio is used to solve the problem of predicting the decay rate from the proposed model that can be generated by this transient region in a way that corrects the boundary condition, $\hat{\tilde{w}}_0$. The length of the transient region is expected to be affected by viscosities, flow speed, and the shape of swirler like vane thickness and vane angle etc. There is a need for further studies on the transient region.

In the case of a swirl injecting pipe with a variable cross-sectional area, the change of the swirl number is more severe than the case of a straight pipe. Therefore, when using this type of swirl injectors, the more careful selection should be needed to obtain the desired swirl number in the burner inlet. It is difficult to simulate all the swirlers individually even if the RANS simulation is performed. This is because a large amount of computation is required for the acceptable calculation even in the RANS simulation, as shown in the grid test in this study. Thus, it is expected that the proposed model of variation of swirl number is very useful for the selection of appropriate swirler to obtain the desired swirl number in swirl injectors.

Bibliography

[1] DW Bahr. Aircraft turbine engine nox emission abatement. In *Unsteady combustion*, pages 243–264. Springer, 1996.

[2] JM Beer and NA Chigier. *Combustion aerodynamics*. Applied Science Publishers Limited, 1972.

[3] F Chang and VK Dhir. Turbulent flow field in tangentially injected swirl flows in tubes. *International Journal of Heat and Fluid Flow*, 15(5):346–356, 1994.

[4] NA Chigier and A Chervinsky. Experimental investigation of swirling vortex motion in jets. *Journal of Applied Mechanics*, 34(2):443–451, 1967.

[5] NA Chigier and K Dvorak. Laser anemometer measurements in flames with swirl. In *Symposium (International) on Combustion*, volume 15, pages 573–585. Elsevier, 1975.

[6] BR Clayton and YSM Morsi. Determination of principal characteristics of turbulent swirling flow along annuli: Part1: Measurement of time mean parameters. *International journal of heat and fluid flow*, 5(4):195–203, 1984.

[7] BR Clayton and YSM Morsi. Determination of principal characteristics of turbulent swirling flow along annuli: part 2: measurement of turbulence components. *International journal of heat and fluid flow*, 6(1):31–41, 1985.

[8] SM Correa. A review of nox formation under gas-turbine combustion conditions. *Combustion science and technology*, 87(1-6):329–362, 1993.

[9] U Engdar and J Klingmann. Investigation of two-equation turbulence models applied to a confined axis-symmetric swirling flow. In *ASME 2002 Pressure Vessels and Piping Conference*, pages 199–206. American Society of Mechanical Engineers, 2002.

[10] S Eskinazi and H Yeh. *An investigation of fully developed turbulent flow in a curved channel*. Johns Hopkins University Institute for Cooperative Research, 1954.

[11] JH Faler and S Leibovich. Disrupted states of vortex flow and vortex breakdown. *The Physics of Fluids*, 20(9):1385–1400, 1977.

[12] JH Faler and S Leibovich. An experimental map of the internal structure of a vortex breakdown. *Journal of Fluid Mechanics*, 86(2):313–335, 1978.

[13] AA Fejer, Z Lavan, and L Wolf Jr. Measurements of the decay of swirl in turbulent flow. *AIAA Journal*, 7(5):971–973, 1969.

[14] S Fujii, K Eguchi, and M Gomi. Swirling jets with and without combustion. *AIAA J.;(United States)*, 19, 1981.

[15] FC Gouldin, JS Depsky, and SL Lee. Velocity field characteristics of a swirling flow combustor. *AIAA Journal*, 23(1):95–102, 1985.

[16] Y Huang and V Yang. Effect of swirl on combustion dynamics in a lean-premixed swirl-stabilized combustor. *Proceedings of the Combustion Institute*, 30(2):1775–1782, 2005.

[17] Y Huang and V Yang. Dynamics and stability of lean-premixed swirl-stabilized combustion. *Progress in energy and combustion science*, 35(4):293–364, 2009.

[18] S Jakirlic, K Hanjalic, and C Tropea. Modeling rotating and swirling turbulent flows: a perpetual challenge. *AIAA journal*, 40(10):1984–1996, 2002.

[19] AM Jawarneh and GH Vatistas. Reynolds stress model in the prediction of confined turbulent swirling flows. *Journal of Fluids Engineering*, 128(6):1377–1382, 2006.

[20] OC Jones and JCM Leung. An improvement in the calculation of turbulent friction in smooth concentric annuli. *Journal of Fluids Engineering*, 103(4):615–623, 1981.

[21] O Kitoh. Experimental study of turbulent swirling flow in a straight pipe. *Journal of Fluid Mechanics*, 225:445–479, 1991.

[22] F Kreith and OK Sonju. The decay of a turbulent swirl in a pipe. *Journal of Fluid Mechanics*, 22(2):257–271, 1965.

[23] AH Lefebvre. The role of fuel preparation in low-emission combustion. *Transactions-American Society of Mechanical Engineers Journal of Engineering for Gas Turbines and Power*, 117:617–617, 1995.

[24] S Leibovich. Vortex stability and breakdown- survey and extension. *AIAA journal*, 22(9):1192–1206, 1984.

[25] TC Lieuwen and V Yang. Combustion instabilities in gas turbine engines(operational experience, fundamental mechanisms and modeling). *Progress in astronautics and aeronautics*, 2005.

[26] I Michiyoshi and T Nakajima. Fully developed turbulent flow in a concentric annulus. *Journal of nuclear science and technology*, 7(5):354–359, 1968.

[27] Lord Rayleigh. On the dynamics of revolving fluids. *Proceedings of the Royal Society of London. Series A, Containing Papers of a Mathematical and Physical Character*, 93(648):148–154, 1917.

[28] H Reichardt. Vollständige darstellung der turbulenten geschwindigkeitsverteilung in glatten leitungen. *ZAMM-Journal of Applied Mathematics and Mechanics/Zeitschrift für Angewandte Mathematik und Mechanik*, 31(7):208–219, 1951.

[29] CJ Scott. A series solution for decay of swirl in an annulus. *Journal of Applied Mechanics*, 39(1):289–290, 1972.

[30] CJ Scott and KW Bartelt. Decaying annular swirl flow with inlet solid body rotation. *Journal of Fluids Engineering*, 98(1):33–40, 1976.

[31] CJ Scott and DR Rask. Turbulent viscosities for swirling flow in a stationary annulus. *Journal of Fluids Engineering*, 95(4):557–566, 1973.

[32] HJ Sheen, WJ Chen, SY Jeng, and TL Huang. Correlation of swirl number for a radial-type swirl generator. *Experimental thermal and fluid science*, 12(4):444–451, 1996.

[33] W Steenbergen and J Voskamp. The rate of decay of swirl in turbulent pipe flow. *Flow measurement and instrumentation*, 9(2):67–78, 1998.

[34] C Stone and S Menon. Open-loop control of combustion instabilities in a model gas turbine combustor*. *Journal of Turbulence*, 4(20), 2003.

[35] N Syred. A review of oscillation mechanisms and the role of the precessing vortex core (pvc) in swirl combustion systems. *Progress in Energy and Combustion Science*, 32(2):93–161, 2006.

[36] N Syred and JM Beer. Combustion in swirling flows: a review. *Combustion and flame*, 23(2):143–201, 1974.

[37] V Tangirala, RH Chen, and James F Driscoll. Effect of heat release and swirl on the recirculation within swirl-stabilized flames. *Combustion Science and Technology*, 51(1-3):75–95, 1987.

[38] FL Wattendorf. A study of the effect of curvature on fully developed turbulent flow. In *Proceedings of the Royal Society of London A: Mathematical, Physical and Engineering Sciences*, volume 148, pages 565–598. The Royal Society, 1935.

[39] FM White. *Fluid mechanics*. McGraw-Hill, 7 edition, 2011.

[40] S Yao and T Fang. Analytical solutions of laminar swirl decay in a straight pipe. *Communications in Nonlinear Science and Numerical Simulation*, 17(8):3235–3246, 2012.

초록

Lean-premixed combustion을 사용하는 gas turbine combustors들은 많은 경우에 flame stabilization을 위한 유동특성인 Central-toiroidal recirculation zone (CTRZ)를 생성하기 위해 Swirling flow를 이용한다. CTRZ의 유동특성들, 특히 그 volume, 들은 combustor inlet (혹은 swirl injector의 끝부분)의 swirl number로 예측 할 수 있다. 본 연구에서는 swirl injecting pipe의 끝 부분에서의 swirl number를 예측하기 위한 새로운 수치적 모델이 제안되었다. 특히 기존의 식들이 제대로 적용되지 못하는 단면적의 변화가 있는 swirl-injector pipe에 대해서도 적용될 수 있는 모델이다. 먼저 swirl decay rate를 예측할 수 있는 수치적인 모델이 swirl injecting pipe의 끝 부분에서의 swirl number를 예측하기 위해 유도되었다. 이 모델은 조심히 설계된 CFD simulations와 validation을 거쳤다. validation의 결과 제안된 모델은 CFD simulation의 결과와 잘 일치하였다. Chapter 4에서는 swirl decay rate에 영향을 줄 수 있는 여러 인자들을 변경해가면서 그것이 decay rate of swirl 에 어떠한 영향을 주는지를 분석하였다. 분석 결과, initial swirl intensity가 작을수록 그리고 inlet Reynolds number가 클수록 swirl decay rate는 작아지는 것을 모델을 통하여 확인하였다. 또한 straight annular pipe에서는 swirl decay rate을 최소화 할 수 있는 γ값이 존재하는것을 제안된 모델을 통하여 확인하였다. 이 값은 0.35 정도로 예측된다. swirl number의 변화를 예측하는 제안된 모델은 swirl injector에서 원하는 swirl number를 얻기위한 swirler의 선택을 하는데에 큰 유용성을 지닐 것으로 생각된다.

주요어: Swirl number, Decay rate of swirl, Swirl injector, Swirl-stabilized burner
학번: 2015-20758